An Ocean Scatter Propagation Model for Aeronautical Satellite Communication Applications

K.W. Moreland
Communications Research Centre
3701 Carling Ave., Ottawa, Ontario
K2H 8S2, Canada
Phone: 613-990-8287, FAX: 613-990-7987

ABSTRACT

In this paper an ocean scatter propagation model, developed for aircraft-to-satellite (aeronautical) applications, is described. The purpose of the propagation model is to characterize the behaviour of sea reflected multipath as a function of physical propagation path parameters. An accurate validation against the theoretical far-field solution for a perfectly conducting sinusoidal surface is provided. Simulation results for typical L-band aeronautical applications with low complexity antennas are presented.

INTRODUCTION

For L-band oceanic mobile satellite communications, sea reflected multipath is the most significant propagation component, especially when relatively low gain, non-directive antennas are employed. A propagation model is required to characterize the behaviour of sea reflected multipath as a function of the elevation angle to the satellite, aircraft altitude, sea state (surface roughness), aircraft antenna characteristics, aircraft velocity, and signal polarization.

Evaluating the electromagnetic field scattered by a rough surface is an extremely difficult problem. Most theoretical approaches are based on the Helmholtz surface integral, with the electric field on the surface assumed to match that present on a tangent plane at that point [1]. In general, complicated integrals that are difficult to solve are obtained.

In many theoretical treatments, attention is restricted to perfectly conducting surfaces in order to simplify the scattering solution. In the perfectly conducting case, the surface reflection coefficient has unity magnitude, independent of grazing angle. This is not appropriate for the sea surface, as is evident from the behaviour of the reflection coefficients at L-band shown in Figure 1. In most theoretical treatments, shadowing and blockage by the surface is ignored for mathematical tractability. Unfortunately, this makes low elevation angle scatter predictions suspect. The propagation model described in this paper incorporates the variability of the surface reflection coefficient as well as shadowing and blockage effects.

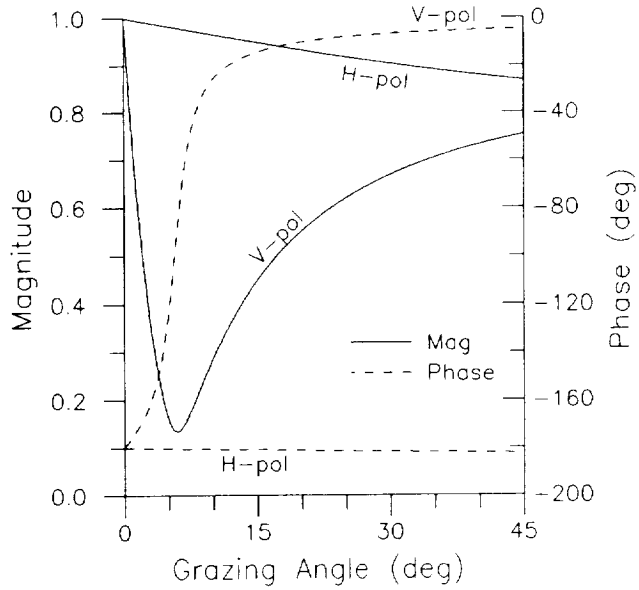

Figure 1: Sea surface reflection coefficients at L-band (λ_c = 0.2 m).

DESCRIPTION OF THE PHYSICAL PROPAGATION MODEL

A simplified view of the physical model that was implemented as a computer simulation is provided in Figure 2. Along the azimuthal direction to the satellite, a rough wave profile $z_w(x)$ is superimposed on a curved earth surface,

$$z_s(x) = z_w(x) - \frac{x^2}{2a_e} \qquad (1)$$

where a_e is the radius of the earth.

It is assumed the waveheight does not vary perpendicular to the azimuthal direction. The wave profile is described by a sum of random phase sinusoidal components of sufficient number to give reasonable agreement with tabulated sea state data. A summary of the wave profile model and appropriate sea state indices is provided in Appendix A.

The initial task in the determination of the scatter signal received at the aircraft antenna is the identification of the surface regions making the most significant contributions. These are the regions about the "specular" points, which geometrically reflect rays to the receiver (see Figure 2). Locating specular points involves finding the values of x where

$$\theta(x) = \beta(x) \qquad (2)$$

with

$$\theta(x) = \tan^{-1}\left\{\frac{z_o - z_s(x)}{x - x_o}\right\} \qquad (3)$$

$$\beta(x) = E - 2\,\varepsilon(x) \qquad (4)$$

$$\varepsilon(x) = \tan^{-1}\left\{\frac{dz_s(x)}{dx}\right\} \qquad (5)$$

$$\alpha(x) = E - \varepsilon(x) = \frac{E + \beta(x)}{2}\,. \qquad (6)$$

Here, $\varepsilon(x)$ denotes the incline of the tangent plane to the surface, $\beta(x)$ is the angle of the reflected ray, $\alpha(x)$ is the local grazing angle, the co-ordinates of the antenna are (x_o,z_o) and E is the elevation angle. The specular point search procedure is extremely computationally demanding for aeronautical applications (i.e. the active scattering region extends to the horizon range of the aircraft). An attractive feature of the simulation model is the exclusion of scattering facets where the specular point is blocked by the wave profile.

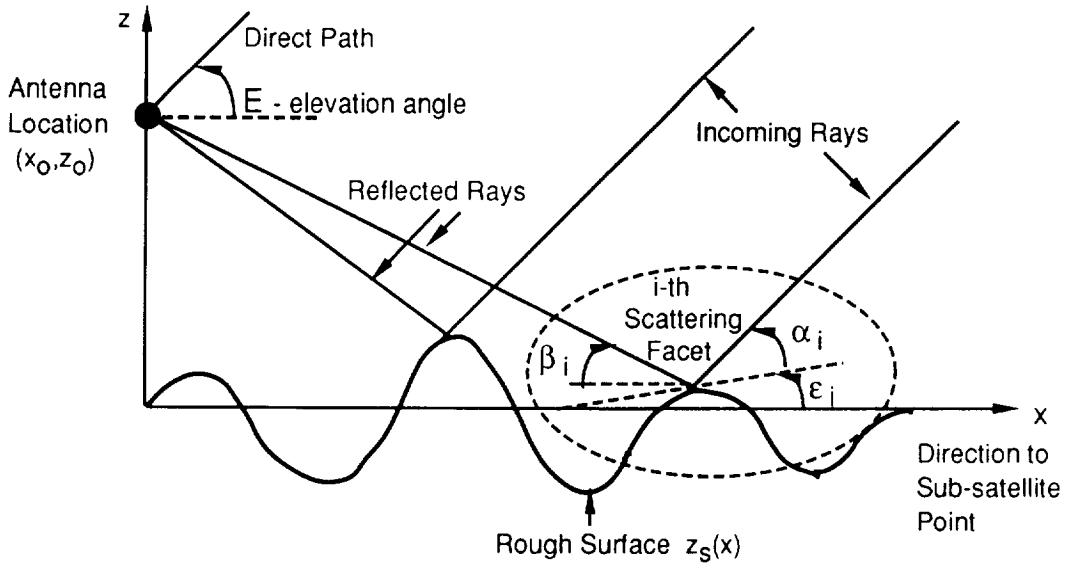

Figure 2 : Propagation model geometry

In the propagation simulation, unmodulated transmissions are considered and the H-pol and V-pol components are treated separately. The scatter signal from each contributing surface facet is accurately determined. This is accomplished by incorporating the variability of the surface reflection coefficient, aircraft antenna gains, as well as the divergence and phase shift resulting from scattering from curved surface facets. That is,

$$S_H(i) = \Gamma_H(\alpha_i)\ e^{-j\phi_i} G_H(B_A - \beta_i)\ A_i \qquad (7)$$

$$S_V(i) = \Gamma_V(\alpha_i)\ e^{-j\phi_i} G_V(B_A - \beta_i)\ A_i \qquad (8)$$

where Γ_H, Γ_V and G_H, G_V denote the surface reflection coefficients and mobile antenna gains for H-pol and V-pol, B_A is the aircraft banking angle (positive towards the surface), ϕ_i is the scatter path phase shift (relative to the direct path), A_i is the signal attenuation and phase shift factor, and β_i and α_i are the reflection and grazing angles, respectively.

The scatter path phase shift can be expressed as

$$\phi_i = \frac{2\pi\, r_i\,(1 - \cos(E+\beta_i))}{\lambda_c} \qquad (9)$$

where r_i is the distance between the antenna and the scattering facet and λ_c is the carrier wavelength.

An appropriate signal attenuation and phase shift factor for the aeronautical application, derived in Appendix C of [2], is

$$A_i = \begin{cases} \left(1 + \frac{r_i}{f_i}\right)^{-1/2} & \text{for convex facets} \\ j\left(\frac{r_i}{f_i} - 1\right)^{-1/2} & \text{for concave facets} \end{cases} \qquad (10)$$

where

$$f_i = \frac{r_c}{2}\sin(\alpha_i) \qquad (11)$$

$$r_c = \left|\frac{(1 + z_s'(x_i)^2)^{3/2}}{z_s''(x_i)}\right| \qquad (12)$$

Here, f_i is the focal length of the curved facet and r_c is the surface radius of curvature. For aeronautical applications, the magnitude of A_i is equivalent to the standard ray-optics divergence factor.

The overall scatter signals for each polarization are given by the superposition of the individual components from each contributing surface facet. These signals can be subsequently combined to account for circular and elliptical polarizations. To give some appreciation for the complexity of the aeronautical propagation simulation, there are in excess of 10,000 contributing facets for an aircraft altitude of 9.1 km, an elevation angle of 10°, and rough surface conditions.

AN IMPORTANT VALIDATION OF THE SIMULATION SOLUTION

For perfectly conducting, sinusoidal surfaces, the far-field Helmholtz integral solution is provided in Section 4.3 of [1]. The received electric field can be expressed as a scaled version of the field that would have been present in the absence of surface roughness. The scale factor ρ is a function of the angle of incidence of the incoming radiation and the scattering direction under consideration. Restricting attention to the specular direction, the theoretical scale factor can be expressed as

$$\rho_{theory} = \left|J_0\left(\frac{\phi_d}{2}\right)\right| \qquad (13)$$

where ϕ_d is the phase difference between the crest and trough specular paths, and $J_0(\cdot)$ is the Bessel function of the first kind of order zero.

The scale factor obtained with the simulation model (p.61 of [2]) is

$$\rho_{sim} = \sqrt{\frac{2}{\pi\left(\frac{\phi_d}{2}\right)}}\left|\cos\left(\frac{\phi_d}{2} - \frac{\pi}{4}\right)\right| \qquad (14)$$

The excellent agreement between the theoretical and simulation solutions for rough surface conditions $\left(\phi_d > \frac{\pi}{2}\right)$ is evident in Figure 3.

SIMULATION RESULTS

Some L-band (f_c=1.5 GHz) aeronautical simulation results for a low complexity crossed-slot antenna are presented in this section. The antenna pattern considered is presented in Figure 4. For rough surface conditions, it has been confirmed that the multipath process can be accurately modelled as a Rayleigh fading process [2]. Given the large number of contributing surface facets, this is not a surprising result. With the addition of a direct path component, a Rician channel model is appropriate for aeronautical applications. The average interference level and behaviour of the second order statistics of the multipath process are required to characterize the fading aeronautical channel.

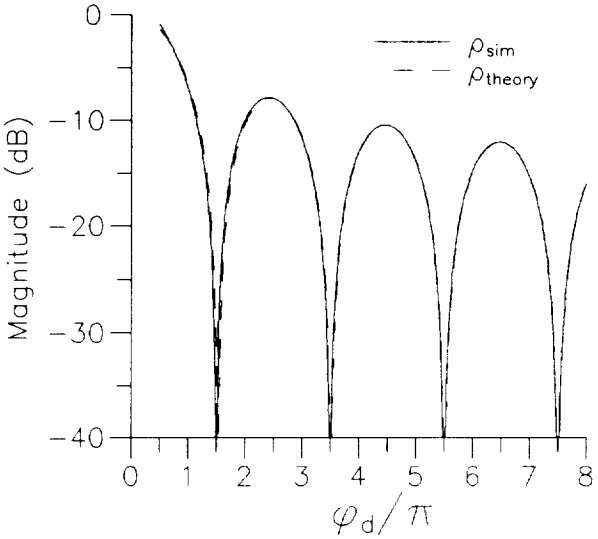

Figure 3 : Simulation and theoretical reflection factors for perfectly conducting sinusoidal surfaces.

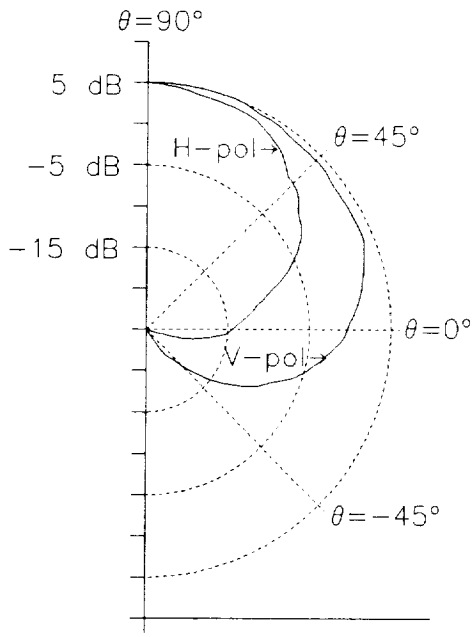

Figure 4 : Crossed-slot antenna pattern

Table 1 summarizes results in terms of signal to interference ratio (S/I) as a function of elevation angle for the crossed-slot and reference omni-antenna patterns. The aircraft altitude was 9.1 km and the surface conditions were rough (sea state index SS4(ii)). The superiority of circular polarization (C-pol) is evident in Table 1. This is a consequence of the polarization sense reversal that a surface imparts on a scattered signal, which is discriminated against by the receiving antenna.

For a circularly polarized crossed-slot antenna, it is evident that S/I is not very sensitive to elevation angle, and the values are excellent, exceeding 20dB. At low elevation angles, the crossed-slot antenna discriminates against H-pol multipath (see Figure 4), while the surface discriminates against V-pol multipath (see Figure 1). With S/I values this high, ocean scatter will

Elevation Angle	S/I [dB] For		
	H-pol	V-pol	C-pol
31°	24.6 (1.2)	16.9 (3.9)	21.6 (17.9)
20°	14.9 (1.0)	15.7 (5.9)	20.4 (13.6)
15°	11.9 (1.6)	16.5 (8.0)	21.3 (12.4)
10°	10.4 (2.7)	18.8 (11.3)	22.9 (11.7)
5°	11.2 (5.2)	21.0 (16.2)	22.9 (12.5)

(Values in parenthesis for an omni-antenna)

Table 1: S/I as a function of elevation angle for an aircraft altitude of 9.1 km and SS4(ii) surface conditions.

not have a severe impact on data communications integrity. Even for an omni-antenna, the S/I values are higher than 10 dB for circular polarization.

The simulation results presented in Table 2 demonstrate that S/I is not very sensitive to sea state and antenna height. The largest difference between the SS3 and SS5(i) results is only 0.7 dB, while the biggest discrepancy between the results for antenna heights of 9.1 km and 5 km is only 0.4 dB. A slight trend of increasing scatter power as the surface gets smoother (decreasing sea state) and as the aircraft altitude is lowered is noticed.

The power spectrum of the multipath process, commonly referred to as the Doppler spectrum, conveys information about the second order statistics of the fading process. An example Doppler spectrum for an elevation angle of 10° is presented in Figure 5. The most striking feature is the asymmetry. This can be theoretically justified (Appendix E of [2]), although the explanation is too lengthy to be presented here. The following relationship between Doppler spread D_{10} (Hz), horizontal airspeed v_x (m/s), and elevation angle E, was derived from simulation results presented in Section 3.2 of [2]:

$$D_{10} = \begin{cases} 0.23\, v_x, & E=10° \\ 0.37\, v_x, & E=15° \\ 1.15\, v_x, & E=31° \end{cases} \qquad (15)$$

Sea State	Aircraft Altitude	S/I [dB] for Polarizations H- pol	V- pol	C-pol
SS3	9.1 km	9.9 (2.4)	18.4 (11.3)	22.7 (11.3)
SS4(ii)	9.1 km	10.4 (2.7)	18.8 (11.3)	22.9 (11.7)
SS5(i)	9.1 km	10.6 (2.8)	18.9 (11.2)	23.0 (11.9)
SS4(ii)	5 km	10.0 (2.5)	18.7 (11.1)	22.5 (11.4)

(Values in parenthesis for an omni-antenna pattern)

Table 2: Effect of sea state and aircraft altitude on S/I for E=10°

Here, D_{10} is the width of the spectral region where the relative Doppler response is above -10 dB. For an aircraft speed of 600 mph, the Doppler spreads are around 60 Hz at low elevation angles (E=10°) and around 300 Hz for intermediate elevation angles (E=31°).

Figure 6 compares simulated H-pol and V-pol scatter power levels for an omni-reference

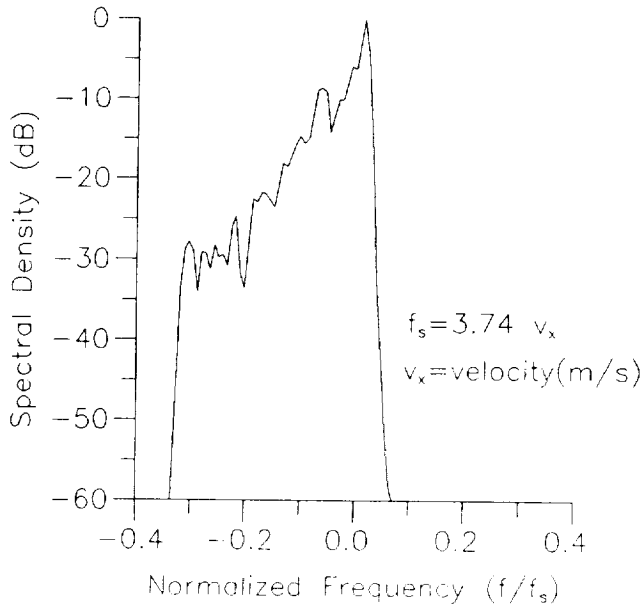

Figure 5 : Doppler spectrum for E=10° and a C-pol omni-antenna.

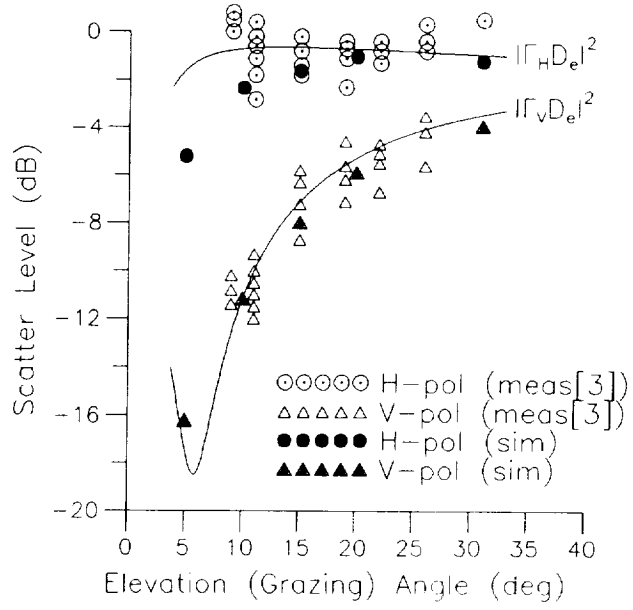

Figure 6 : Measured and simulated scatter power levels for an omni-antenna.

antenna against measurement results from [3] and a simple approximation given by the magnitude squared value of the product of surface reflection coefficient and the divergence factor of the earth [3]. The agreement for elevation angles above 10° is quite good.

APPENDIX A
SURFACE MODEL

The wave profile used in this study is described by a sum of random phase sinusoidal components, with a white bandpass spatial spectrum,

$$z_w(x) = \frac{\sqrt{2}\sigma_z}{\sqrt{N_T}} \sum_{k=-N}^{N} \cos(2\pi u_k x + \theta_k)$$

where $N_T=2N+1$ is the number of sinusoidal components, θ_k is a uniformily distributed random phase, $u_k=u_o(1+\frac{k\gamma}{N_T})$, $\gamma = 1.344$, and $u_o = (1.0726\ \Lambda)^{-1}$. The dependence of the rms waveheight σ_z and average sea wavelength Λ on sea state is provided in Table A.1 for a few representative cases.

For the simulation runs, N_T was chosen to be 21. With the above parameter values, the wave profile generated by this model is approximately Gaussian with a correlation distance of $\Lambda/4.44$. According to [4], this is a realistic model for a 1-dimensional cross-section of the ocean surface.

Sea State Index	RMS Waveheight (Meters)	Average Sea Wavelength (Meters)
3	0.35	22.3
4(i)	0.525	30.75
4(ii)	0.61	34.3
5(i)	0.76	41.9
5(ii)	0.92	48.8

Table A.1: Representative sea state table

A nice feature of this surface model is that derivatives, which are required in the geometrical search for specular points and radius of curvature computations, are easily determined.

REFERENCES

[1] P. Beckmann and A. Spizzichino, "The Scattering of Electromagnetic Waves From Rough Surfaces", The MacMillan Company, New York, 1963.

[2] K.W. Moreland, "Ocean Scatter Propagation Models For Aeronautical and Maritime Satellite Communication Applications", Master's Thesis, Faculty of Engineering, Dept. of Systems and Computer Engineering, Carleton University, February 1987.

[3] R.W. Sutton et.al., "Satellite-Aircraft Multipath and Ranging Experiments at L-band", IEEE Trans.Comm, May 1973.

[4] P. Horn et.al., "Theoretical Study of Multipath Effects In An Aeronautical Satellite System", Messerschmitt-Bolkow-Blohm, Contract Report 1064/70CG (RFQ/737) for European Space Research and Technology Centre, Noordwijk, Holland, November 1970, p.127-128.